JOURNAL OF APPLIED POLYMER SCIENCE VOL. 16, PP. 3285-3306 (1972)

Studies on Melt Spinning. II. Analysis of the Deformation and Heat Transfer Processes

RONALD R. LAMONTE and CHANG DAE HAN,
Department of Chemical Engineering, Polytechnic Institute of Brooklyn, Brooklyn, New York 11201

Synopsis

A generalized, empirical equation is proposed which takes into account the dependence of elongational viscosity on both elongation rate and temperature. From this, a mathematical model for simulating the melt spinning process has been developed. The model has been tested against experimentally observed velocity profiles in fibers of polystyrene and high-density polyethylene spun into an isothermal chamber. It has been found that predicted velocity profiles agree well with experimentally observed ones. The mathematical model has been used to predict velocity and temperature profiles in fibers spun into a cooling medium. The simultaneous solution of momentum and energy balance equations by means of a numerical integration scheme has generated important information such as distributions of force components involved in spinning and distributions of the total rate of heat transfer along the spinning way.

INTRODUCTION

In a previous paper,[1] which was the first of this series, the authors presented some experimental measurements of elongational viscosity of several polymers in the molten state. The two main objectives of that study were to experimentally determine the dependence of elongational viscosity on elongation rate, as affected by the molecular structure of the materials, and to isolate the effect of elongation rate from the effect of threadline cooling on elongational viscosity, by performing the spinning experiment isothermally.

However, cooling of threadline is very important in commercial melt spinning, and careful control of the rate of cooling of molten threadlines is very intimately related to producing a desired quality of finished fiber. The rate of cooling, together with the rate of stretching, influences both the degree of molecular orientation and the rate of crystallization. Unfortunately, at present we do not have a clear understanding of the relationships between the rate of stretching and the degree of molecular orientation, and between it and the rate of cooling. Therefore, a rigorous analysis of the melt spinning process is much more complicated than it may appear to be. Complication comes not only from the lack of our understanding of the problem involved with cooling, but also from the very complicated nature of the elongational flow behavior of fiber-forming polymers in the molten state.

Much of the previous studies therefore were concerned with certain aspects of the problems involved in melt spinning. Some[2,3,4] were concerned with the heat transfer between a moving threadline and the coolant; some,[5,6,7] with molecular orientation in a filament as affected by various spinning conditions; others,[1,8] with the deformation of a molten threadline spun into an isothermal chamber; and still others,[9,10,11] with both deformation and heat transfer together. In their analysis of nonisothermal spinning of polyester, Kase and Matsuo[9] assumed that elongational viscosity depends on temperature alone, but not on elongation rate. These authors then determined the temperature dependence of elongational viscosity from the measurements of temperature profiles along the spinline. Unfortunately, they were not able to check the validity of their assumption.

In the present paper, which is the second of this series, we first propose a generalized, empirical equation of elongational viscosity based on the currently available experimental results in the literature. We then present our analysis made recently for simulating nonisothermal melt spinning process. The analysis involves the numerical integration of the momentum and energy balance equations. Computations have been carried out to simulate our recent spinning experiments using low-density polyethylene, high-density polyethylene, and polystyrene.

A GENERALIZED EMPIRICAL EQUATION OF ELONGATIONAL VISCOSITY

Rate Dependence of Elongational Viscosity

Many studies[12–15] have been reported in the literature in which efforts were made to derive theoretical expressions for elongational viscosity using various forms of constitutive equations. It is worth noting that almost all of the theoretical studies assumed constant elongation rate and yet give rate-dependent expressions yielding values of elongational viscosity which increase with elongation rate.

On the other hand, it is not an easy matter to keep the elongation rate constant during an experiment. There are some researchers[16,17] who attempted to control experimental conditions so that constant elongation rate could be realized. However, recent experimental studies[1,8] show that, in melt spinning, elongation rate varies along the spinway. It should be noted that in melt spinning, one is interested in controlling stretch rate rather than elongation rate. In fact, studies of Acierno et al.[8] and Han and Lamonte[1] show that elongation rate may increase or decrease along the spinway, depending on the material being spun, and that elongational viscosity also may increase or decrease with elongation rate or stay constant independent of elongation rate. Figure 1 gives some representative results in the recent paper by Han and Lamonte.[1] Hence, in view of the experimental fact that in melt spinning the assumption of constant elongation rate may not hold, an analysis of the melt spinning process requires a more realistic rate-dependent expression for elongational viscosity.

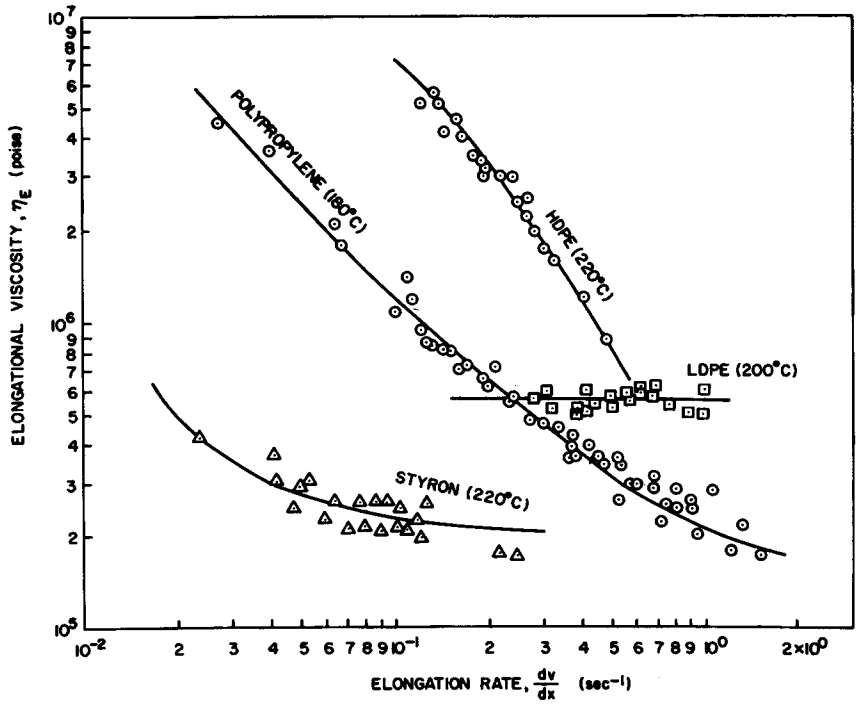

Fig. 1. Plots of elongational viscosity vs. elongation rate of polymer melts under isothermal spinning conditions.

However, a rigorous theoretical analysis of the elongational flow of fiber-forming materials is very difficult, largely for the following two reasons. One is that many of the fiber-forming polymers, if not all, are viscoelastic in the molten state and have large relaxation times. Therefore, a choice of constitutive equation, although somewhat arbitrary, requires the consideration of fairly complicated models. Another is that a correct description of the rheological properties of a material point in the threadline requires the prehistory of deformation of the same material point. It is extremely difficult, if not impossible, to analytically describe all the prior deformation of the material point in question, including that inside the spinnerette holes. The importance of the prehistory of deformation has been very nicely demonstrated in a recent experiment by Chen et al.[19]

In view of the complicated nature of the purely theoretical approach, we propose here a generalized, empirical equation for elongational viscosity:

$$\eta_E = 3\eta_0 \left[a + b \left(\frac{dv_z}{dz} \right)^{q-1} \right] \tag{1}$$

on the basis of the currently available experimental data derived by various investigators.[1,8,16–20] Here, η_0 denotes zero-shear viscosity, dv_z/dz denotes elongation rate, and a, b, and q are constants characteristic of the materials.

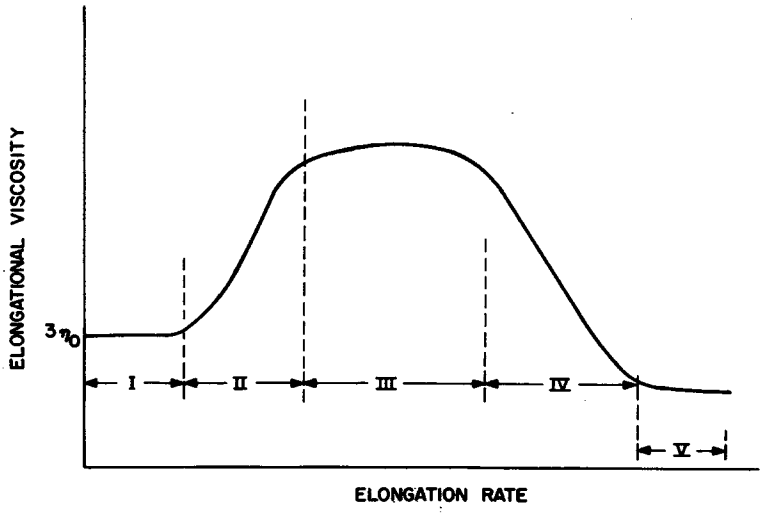

Fig. 2. Schematic of elongational viscosity vs. elongation rate behavior.

Figure 2 gives a schematic representation of eq. (1). Special cases of eq. (1) worth considering are:

Case 1. Setting $a = 1$ and $b = 0$ reduces eq. (1) to

$$\eta_E = 3\eta_0 \tag{2}$$

which is a well-known expression due to Trouton.[21] Equation (2) represents region I in Figure 2.

Case 2. Setting $a = 0$ and taking $b \geq 1$ and $q > 1$ reduces eq. (1) to

$$\eta_E = 3\eta_0 b \left(\frac{dv_z}{dz}\right)^{q-1} \qquad q > 1 \tag{3}$$

which represents region II in Figure 2. It is seen that in region II, η_E increases with elongation rate dv_z/dz.

Case 3. Setting $a = 0$ and $q = 1$ and taking $b > 1$ reduces eq. (1) to

$$\eta_E = 3\eta_0 b > 3\eta_0 \tag{4}$$

which represents region III in Figure 2. It is important to note that in region III, η_E is constant, independent of elongation rate dv_z/dz, but its magnitude is larger than that of $3\eta_0$, the case of a Newtonian fluid.

Case 4. Setting $a = 0$ and taking $b > 1$ and $q < 1$ reduces eq. (1) to

$$\eta_E = 3\eta_0 b \left(\frac{dv_z}{dz}\right)^{q-1} \qquad q < 1 \tag{5}$$

which represents region IV in Figure 2. Note that, although the form of eq. (5) is identical to that of eq. (3), eq. (5) defines elongational viscosity decreasing with elongation rate due to $q < 1$.

Case 5. Setting $b = 0$ and taking $0 < a < 1$ reduces eq. (1) to

$$\eta_E = 3\eta_0 a < 3\eta_0 \tag{6}$$

which represents region V in Figure 2. In region V, η_E is constant again, but its magnitude is smaller than $3\eta_0$, the case of a Newtonian fluid.

It can be seen from the above that other combinations of material constants a, b, and q are also possible. It should be noted also that eq. (1) can be used to represent two regions in Figure 2 instead of one by properly choosing combinations of the material constants. For instance, a choice of $a = 1$, $b > 0$, $q > 1$ represents regions I and II; a choice of $a > 1$, $b > 0$, $q < 1$ represents regions III and IV; and a choice of $0 < a < 1$, $b < 0$, $q < 1$ represents regions IV and V.

A summary of experimental results by several investigators is given in Table I. Depending on the material tested and the experimental technique employed, it was possible to obtain only a part of the entire elongational viscosity curve sketched in Figure 2. Because of limitations of experimental techniques, it may be practically impossible for any single experimental technique to generate the entire η_E curve over a wide range of elongation rates.

TABLE I
A Summary of Experimental Results on the Elongational Viscosity of Polymer Melts by Various Investigators

Material	Investigator	Dependence of η_E on $\dot{\gamma}_E$
Polystyrene	Acierno et al.[8]	decreasing: regions IV and V
	Ballman[16]	constant: region III
	Han and Lamonte[1]	decreasing: regions IV and V
Low-density polyethylene	Cogswell[20]	increasing: region II
	Cogswell[18]	constant: region III
	Han and Lamonte[1]	constant: region III
	Meissner[17]	increasing: region II
High-density polyethylene	Acierno et al.[8]	increasing: region II
	Han and Lamonte[1]	decreasing: region IV
Polypropylene	Han and Lamonte[1]	decreasing: regions IV and V

It is appropriate to note the earlier work by Matovich and Pearson[22] at this point. They contended that eq. (3) enhances spinnability ($q > 1$) while eq. (5) hinders spinnability ($q < 1$). Of course, a criterion of spinnability is somewhat arbitrary. If spinnability is defined as the ability of a material to form a continuous filament, a stretch ratio v_L/v_0 may be a convenient variable to use. Here, v_L/v_0 is the ratio of the take-up velocity to the initial velocity of a threadline. According to this definition, it can be said that the larger the value of v_L/v_0, the more spinnable a material is. It is interesting to note, however, from Figure 1 that three polymers employed in a recent study by Han and Lamonte[1] give rise to $q < 1$ and yet were found quite spinnable. For instance, polypropylene at 180°C was spun at

$v_L/v_0 = 212$ before thread breakage, despite the fact that q is approximately 0.117 over the range of elongation rates 0.04–0.4 sec^{-1}.

Temperature Dependence of Elongational Viscosity

In order to analyze the nonisothermal spinning process, one needs an expression which shows how elongational viscosity varies as melt temperature is changed. Because a threadline gets cooled as it travels through the spinway, we do not, at present, have a clear idea of how the effect of temperature should be incorporated in a theoretical expression for the elongational viscosity of viscoelastic fluids.

On the other hand, one can carry out a well-controlled experimental study which may give some insight into how elongational viscosity would vary as the melt temperature is changed. Very recently, Han and Lamonte[1] have carried out isothermal melt spinning experiments at different melt temperatures and have found that the Eyring-Frankel equation holds for the observed elongational viscosity. It should be noted that the experimental approach of Han and Lamonte[1] is different from that of Kase and Matsuo.[9] The former kept the temperature of the molten threadline constant in a heated chamber of a fixed distance in which the diameter of the threadline was photographically measured. They repeated these measurements at different melt temperatures for each run On the other hand, Kase and Matsuo measured the temperature profiles of a threadline which was being cooled and stretched simultaneously; in an experiment such as that, one cannot separate the temperature effect on the measured elongational viscosity from the stretching effects. In fact, Kase and Matsuo[9] assumed the effect of stretching on the elongational viscosity to be negligibly small compared to the temperature effect. This assumption may not hold in general, and the experience of the authors has indicated it not to be the case in their experiments.

In view of the difficulty of taking care of the temperature effect from a theoretical standpoint, we propose here the following empirical expression:

$$\eta_E = 3\alpha e^{\beta/T}\left[k_1 + k_2\left(\frac{dv_z}{dz}\right)^{q-1}\right] \tag{7}$$

where

$$\begin{aligned} \alpha &= \eta_0(T_0)e^{-E/RT_0} \\ \beta &= E/R \\ E &= E_s + E_e \\ k_1 &= a(T_0) \\ k_2 &= b(T_0) \end{aligned} \tag{8}$$

Here, E is the activation energy, determined experimentally, and consisting of two parts: one, the shear flow activation energy E_s, which comes from

the zero shear viscosity; and the other, the elongational flow activation energy E_ϵ; and k_1 and k_2 are the values of a and b, defined in eq. (1), evaluated at some reference temperature T_0. In proposing eq. (7), we have assumed that the two constants a and b in eq. (1) are given by the Eyring-Frankel equation under the elongational flow field:

$$a(T) = a(T_0)e^{E_\epsilon/R(1/T-1/T_0)} \tag{9}$$

$$b(T) = b(T_0)e^{E_\epsilon/R(1/T-1/T_0)}. \tag{10}$$

In the analysis to follow we shall use eq. (7), together with the momentum and energy balance equations, in order to simulate the nonisothermal melt spinning process.

ANALYSIS OF NONISOTHERMAL MELT SPINNING

Referring to Figure 3, we shall consider region II, in which a molten threadline is stretched and cooled between the spinnerette and the take-up device. We can then write the following differential equations using cylindrical coordinates:

Equation of continuity:

$$\frac{1}{r}\frac{\partial}{\partial r}(\rho r v_r) + \frac{\partial}{\partial z}(\rho v_z) = 0 \tag{11}$$

r-Component equation of motion:

$$\rho\left(v_r\frac{\partial v_r}{\partial r} + v_z\frac{\partial v_z}{\partial z}\right) = \frac{1}{r}\frac{\partial}{\partial r}(rS_{rr}) - \frac{S_{\theta\theta}}{r} + \frac{\partial S_{rr}}{\partial z} \tag{12}$$

z-Component equation of motion:

$$\rho\left(v_r\frac{\partial v_z}{\partial r} + v_z\frac{\partial v_z}{\partial z}\right) = \rho g + \frac{1}{r}\frac{\partial}{\partial r}(rS_{rz}) + \frac{\partial S_{zz}}{\partial z} \tag{13}$$

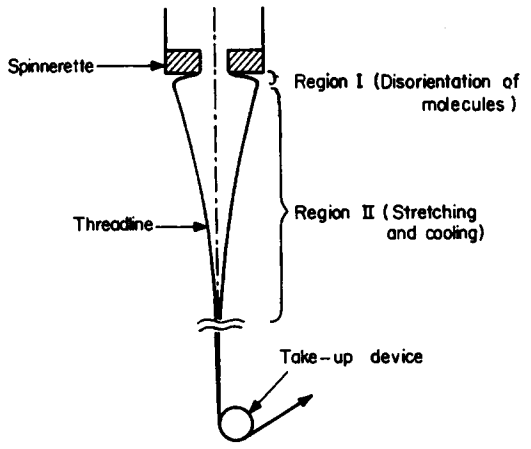

Fig. 3. Schematic of melt spinning process.

Equation of energy:

$$\rho C_v \left(v_r \frac{\partial T}{\partial r} + v_z \frac{\partial T}{\partial z} \right) = -\frac{1}{r} \frac{\partial}{\partial r} (r q_r) - \frac{\partial q_z}{\partial z} + \left[S_{rr} \frac{\partial v_r}{\partial r} + S_{\theta\theta} \frac{v_r}{r} + S_{zz} \frac{\partial v_z}{\partial z} + S_{rz} \left(\frac{\partial v_z}{\partial r} + \frac{\partial v_z}{\partial z} \right) \right] \quad (14)$$

In eqs. (11)–(14), S_{ij} are the ijth components of stress; ρ is the fluid density; C_v is the heat capacity, g is the gravitational constant; q_r and q_z are the r- and z-components of heat flux, respectively; v_r and v_z are r- and z-components of velocity, respectively; and T is the fluid temperature.

If we now make the following simplifying assumptions: (a) v_z depends on z only, i.e., $v_z = v_z(z)$; (b) T depends on z only, i.e., $T = T(z)$; (c) q_z is negligibly small; (d) C_v is independent of T; and (e) the viscous heat dissipation is negligible, which makes the bracketed term on the right-hand side of eq. (14) drop out, then eqs. (13)–(14) reduce to

$$\rho v_z \frac{dv_z}{dz} = \rho g + \frac{1}{r} \frac{\partial}{\partial r} (r S_{rz}) + \frac{\partial S_{zz}}{\partial z} \quad (15)$$

$$\rho C_v v_z \frac{dT}{dz} = -\frac{1}{r} \frac{\partial}{\partial r} (r q_r). \quad (16)$$

We shall assume further that the following boundary conditions reasonably describe the physical situation under consideration:

(i) at $z = 0$, $v_z(0) = V_0$, $T(0) = T_0$ (17)

(ii) at $z = L$, $v_z(L) = V_L$ (18)

(iii) at $r = R(z)$, $q_r[R(z)] = h(T - T_a) + \lambda\epsilon(T^4 - T_a^4)$ (19)

in which λ is the Stefan-Boltzman constant, and ϵ is the emissivity.

Now, multiplying both sides of eq. (15) by rdr and integrating the resulting equation from $r = 0$ to $r = R(z)$, we obtain

$$\frac{\rho v_z R^2}{2} \frac{dv_z}{dz} = \rho g \frac{R^2(z)}{2} + R[S_{rz} - R' S_{zz}]_{r=R(z)} + \frac{d}{dz} \int_0^{R(z)} S_{zz} r dr \quad (20)$$

where R' is the derivative of $R(z)$ with respect to z. Noting that the stresses at the surface $r = R(z)$ are given by

$$[S_{rz} - R' S_{zz}]_{r=R(z)} = -F_d - 2H\sigma R' \quad (21)$$

in which F_d is the drag force, σ is the surface tension force, and H is the radius of curvature given by

$$H = \frac{1}{R[1 + (R')^2]^{1/2}} - \frac{R''}{[1 + (R')^2]^{3/2}} \quad (22)$$

eq. (20) may be rewritten as:

$$\frac{1}{2}\rho v_z R^2 \frac{dv_z}{dz} = \frac{1}{2}\rho g R^2 + R[-F_d - 2H\sigma R'] + \frac{d}{dz}\left[\frac{1}{2} S_{zz} R^2\right]. \quad (23)$$

Again, multiplying both sides of eq. (16) by rdr and integrating the resulting equation from $r = 0$ to $r = R$ gives

$$\frac{1}{2}\rho C_v R^2 \frac{dT}{dz} = -R\{h(T - T_a) + \lambda\epsilon(T^4 - T_a^4)\} \quad (24)$$

in which the boundary condition of eq. (19) was used.

We can now further simplify eqs. (23) anc (24) by making use of the continuity condition

$$Q = \rho\pi R^2 v_z \quad (25)$$

where Q is the mass flow rate. Using eq. (25) to eliminate R, eqs. (23) and (24) reduce to

$$v_z \frac{dv_z}{dz} = g + v_z \frac{d}{dz}\left(\frac{S_{zz}}{\rho v_z}\right) + 2\sqrt{\frac{\pi v_z}{\rho Q}}\{-F_d - 2H\sigma R'\} \quad (26)$$

$$\frac{dT}{dz} = -\frac{2}{C_v}\sqrt{\frac{\pi}{\rho Q v_z}}\{h(T - T_a) + \lambda\epsilon(T^4 - T_a^4)\}. \quad (27)$$

Equations (26)–(27) are general working equations whose solutions will describe the velocity and temperature profiles of a threadline along the spinway. It should be noted, however, that solution of eqs. (26) and (27) requires the specification of S_{zz} in terms of the elongation rate dv_z/dz.

Before we present our computational results for specific polymer systems chosen for the melt spinning experiment, let us consider a few special cases of eqs. (26) and (27).

Case 1. Isothermal spinning with Newtonian fluid, where the drag force is negligible: In this situation, the tensile stress S_{zz} is represented by

$$S_{zz} = 3\eta_0 \left(\frac{dv_z}{dz}\right). \quad (28)$$

Using eq. (28) and $F_d = 0$ in eq. (26) gives

$$v_z \frac{dv_z}{dz} = g - \frac{3\eta_0}{\rho}\frac{1}{v_z}\left(\frac{dv_z}{dz}\right)^2 + \frac{3\eta_0}{\rho}\frac{d^2 v_z}{dz^2} - 4\sqrt{\frac{\pi v_z}{\rho Q}} H\sigma R'. \quad (29)$$

Case 2. Isothermal spinning with a power law-type of elongational viscosity, represented either by eq. (3) ($q > 1$) or eq. (5) ($q < 1$): In this situation the tensile stress S_{zz} is represented by

$$S_{zz} = 3\eta_0 b \left(\frac{dv_z}{dz}\right)^{q-1} \frac{dv_z}{dz}. \quad (30)$$

If we further assume $F_d = 0$, the use of eq. (30) in eq. (26) gives

$$v_z \frac{dv_z}{dz} = g - \frac{3\eta_0 b}{\rho} \frac{1}{v_z} \left(\frac{dv_z}{dz}\right)^{q+1} + \frac{3\eta_0 bq}{\rho} \left(\frac{dv_z}{dz}\right)^{q-1} \frac{d^2v_z}{dz^2} - 4\sqrt{\frac{\pi v_z}{\rho Q}} H\sigma R'. \tag{31}$$

Note that eq. (31) reduces to eq. (29) when $b = 1$ and $q = 1$, which is as expected, in view of the fact that eq. (30) similarly reduces to eq.(28).

Matovich and Pearson[22] have considered the above two cases of isothermal spinning. However, their equations contain an error in the expression of the surface tension term, arising from their erroneous expression for the axial radius of curvature. Their eq. (8) should read the same as our eq. (22).

We now return to considering the situation of nonisothermal spinning, for which we assume the following: (a) The surface tension force is negligible (i.e., $\sigma = 0$). (b) The drag force is given by the expression due to Sakiadis[23]:

$$F_d = \frac{0.843}{\pi R^2} (\rho^0/\rho) Q v_z \left[\frac{\pi \rho \nu^0 (L - z)}{Q}\right]^{0.915} \tag{32}$$

where ρ^0 and ν^0 are the density and kinematic viscosity of ambient air, respectively; ρ is the density of the threadline being cooled (i.e., ρ varies with temperature); and L is the distance between the spinnerette face (more rigorously speaking, at a position where the maximum die swell occurs) and the position where deformation of the threadline ceases. (c) The heat transfer coefficient h is represented by the expression due to Kase and Matsuo[9]:

$$h = 0.21(1 + K)k^0 \sqrt{\frac{\pi \rho v_z}{q}} \left(\frac{2}{\nu_0}\right)^{0.334} \left(\frac{\rho Q v_z}{\pi}\right)^{0.117} \tag{33}$$

where k^0 is the thermal conductivity of ambient air and K is an adjustable parameter which depends on the direction of air flow with respect to the threadline and also on the fiber-forming polymer. (d) The tensile stress S_{zz} is given by

$$S_{zz} = 3\alpha e^{\beta/T} \left[k_1 + k_2 \left(\frac{dv_z}{dz}\right)^{q-1}\right] \frac{dv_z}{dz} \tag{34}$$

where α, β, k_1, and k_2 are as defined in eqs. (8). Based on the above assumptions, eqs. (26) and (27) may be rewritten as follows:

$$\begin{aligned} v_z \frac{dv_z}{dz} = g &+ \frac{3\alpha}{\rho} e^{\beta/T} \left[k_1 + k_2 q \left(\frac{dv_z}{dz}\right)^{q-1}\right] \frac{d^2v_z}{dz^2} \\ &- \frac{3\alpha\beta}{\rho T^2} e^{\beta/T} \left[k_1 + k_2 \left(\frac{dv_z}{dz}\right)^{q-1}\right] \frac{dv_z}{dz} \frac{dT}{dz} \\ &- \frac{3\alpha}{\rho} e^{\beta/T} \left[k_1 + k_2 \left(\frac{dv_z}{dz}\right)^{q-1}\right] \left[\frac{1}{v_z} \frac{dv_z}{dz} + \frac{1}{\rho} \frac{d\rho}{dT} \frac{dT}{dz}\right] \frac{dv_z}{dz} \\ &- 1.686\rho^0 \sqrt{\frac{\pi}{Q\rho}} v^{5/2} \left[\frac{\pi \rho \nu_0 (L - z)}{Q}\right]^{0.915} \end{aligned} \tag{35}$$

$$\frac{dT}{dz} = -\frac{2}{C_v}\sqrt{\frac{\pi}{\rho Q v_z}}\left\{0.21(1+K)k^0\sqrt{\frac{\pi\rho v_z}{Q}}\left(\frac{2}{\nu_0}\right)^{0.334}\left(\frac{\rho Q v_z}{\pi}\right)^{0.117}(T - T_a) + \lambda\epsilon(T^4 - T_a^4)\right\}. \quad (36)$$

Now, it is seen that simultaneous solution of eqs. (35) and (36), with the aid of boundary conditions (17) and (18), would predict the distributions of fiber velocity v_z and temperature T along the spinning way z. Since an analytical solution of eqs. (35) and (36) does not appear to exist, one has to resort to numerical techniques. Details of the numerical technique employed in the present study will be given below when the representative results of theoretical predictions will be presented.

RESULTS AND DISCUSSION

Having presented a mathematical model for the simulation of the melt spinning process, we shall first make a comparison of the theoretically predicted and experimentally observed velocity profiles in fibers spun into an isothermal chamber. And then, we shall further discuss predictions of velocity and temperature profiles in nonisothermal spinning.

Simulation of the Isothermal Melt Spinning Process

Figures 4 and 5 give some representative results of the velocity profiles in high-density polyethylene and polystyrene fibers, respectively. The expermental techniques employed in the determination of fiber velocities has been described in our previous paper.[1] It is seen in Figures 4 and 5 that agreement between the experimentally observed and theoretical predicted velocity profiles are quite satisfactory. Some details of the predicted velocity profiles are worth elaborating on.

First, as may be noted from Figure 1, high-density polyethylene and polystyrene behave differently in the elongational flow field. That is, the elongational viscosity of high-density polyethylene follows eq. (5) (i.e., region IV in Fig. 2), and the elongational viscosity of polystyrene follows eq. (1) (i.e., regions IV and V in Fig. 2). Therefore, material constants in the proposed generalized, empirical model, eq. (7), had to be determined for the materials concerned. This was done by obtaining the best fit of the model, eq. (7), to experimental data (see Fig. 1) by means of a nonlinear least-squares method. Table II gives a summary of the numerical values of material constants for high-density polyethylene, low-density polyethylene, and polystyrene.

Second, although in this particular instance we were interested, for comparison purposes, in obtaining velocity profiles in an isothermal chamber of about 10-cm length, we solved both eqs. (35) and (36) stepwise; that is, eq. (35) from $z = 0.0$ to $z = 10.0$ cm, and then eqs. (35) and (36) from $z = 10.0$ to $z = L$ cm. Here, L is the distance at which the deformation of a fiber is assumed to cease. This definition can be somewhat ambiguous for poly-

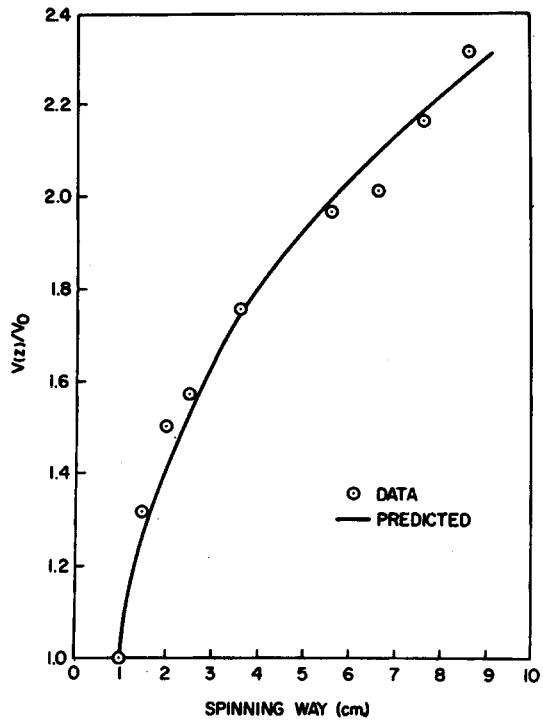

Fig. 4. Comparison of experimentally observed and theoretically predicted velocity profiles in high-density polyethylene fibers. Spinning conditions: Q = 0.025 g/sec; V_0 = 1.598 cm/sec; V_L/V_0 = 8.16; T_0 = 220°C; spinneret diameter, 1.0 mm.

mers which can undergo considerable cold drawing. In the present study, however, L has been taken as the solidification point of the polymer. It should be noted that eqs. (35) and (36) define a boundary value problem, because another boundary condition at $z = 0$, e.g., dv_z/dz at $z = 0$, was not available from experiment. However, we have considered the boundary value problem as an initial value problem, strictly from a computational point of view. In other words, in carrying out numerical integration of eqs. (35) and (36), we first guessed dv_z/dz at $z = 0$ and

TABLE II
Values of Material Constants in Eq. (7) for Materials Investigated

Material	Sample code	Temp., °C	α	β	k_1	k_2	q
High-density polyethylene	HDPE (DMDJ4309)	220	2.54×10^4	7.8×10^3	0.0	0.0017	−0.359
Low-density polyethylene	LDPE (PEP 211)	200	48.5	5.67×10^3	1.0	0.0	—
Polystyrene	Styron	220	0.023	1.44×10^4	0.861	0.462	0.0775

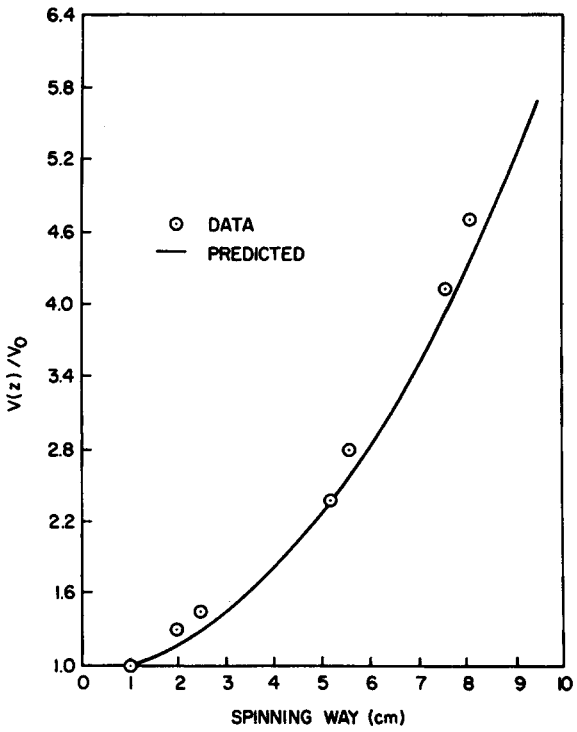

Fig. 5. Comparison of experimentally observed and theoretically predicted velocity profiles in polystyrene fibers. Spinning conditions: Q = 0.045 g/sec; V_0 = 2.17 cm/sec; V_L/V_0 = 501.7; T_0 = 220°C; spinneret diameter, 1.0 mm.

proceeded to integrate forward to calculate v_z at $z = L$, V_L. The computed value of V_L was compared with the specified one, and the numerical integration was repeated until the comparison was satisfactory within a prescribed error limit. Numerical integration was carried out using the fourth-order Runge-Kutta predictor-corrector method, and the "shooting" technique advanced by Keller[24] for successively guessing values of dv_z/dz at z = 0. Details of the computational procedure used are given in Figure 6 in a form of flow diagram.

Figure 7 gives computed temperature profiles of high-density polyethylene and polystyrene fibers, spun into an isothermal chamber 10 cm long and into the ambient. The flat portion in Figure 7 represents the isothermal chamber in which no cooling is supposed to occur. It is seen that the fiber temperature falls rapidly outside the isothermal chamber.

Simulation of the Nonisothermal Spinning Process

In the absence of the isothermal chamber, eqs. (35) and (36) were numerically integrated from z = 0.0 to $z = L$ by slightly modifying the computational procedure given in Figure 6. Representative results of the prediction

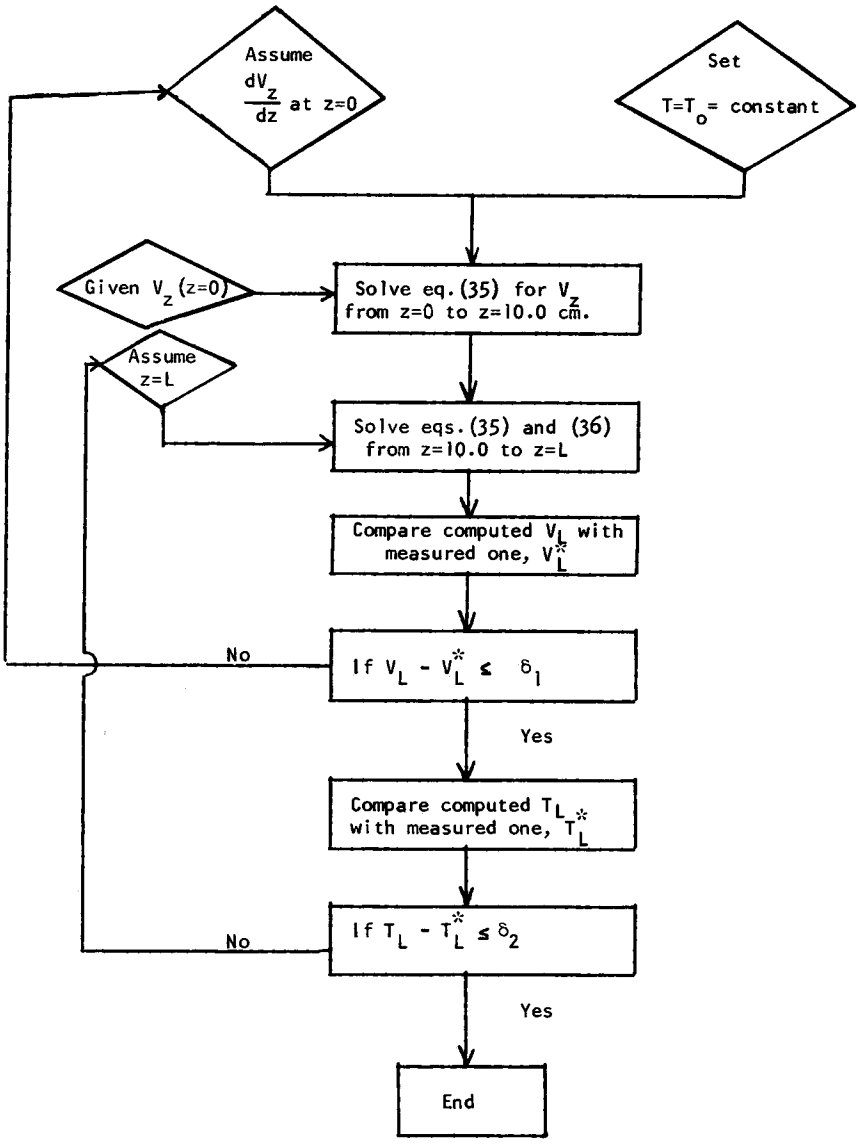

Fig. 6. Flow diagram of the computational scheme.

of fiber velocity profiles are given in Figure 8 for high-density polyethylene, in Figure 9 for low-density polyethylene, and in Figure 10 for polystyrene. Having solved eqs. (35) and (36), we have been able to calculate the distributions of various force components along the spinning way. Table III gives the force distributions in a high-density polyethylene fiber, Table IV, the force distributions in a low-density polyethylene fiber, and Table V, the force distributions in a polystyrene fiber. The calculation of the individual components of force (i.e., the gravitational force F_{grav}, the inertial force F_{inert},

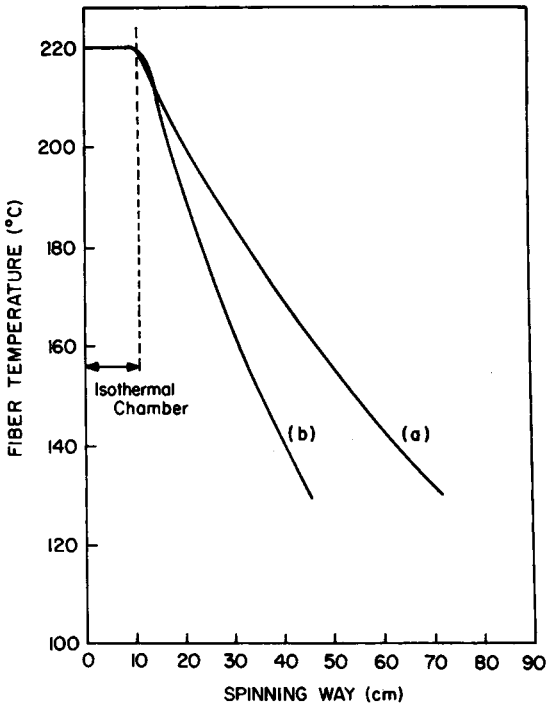

Fig. 7. Predicted temperature profiles in the presence of the isothermal chamber: (a) high-density polyethylene at 220°C, Q = 0.0251 g/sec, V_L/V_0 = 8.16; (b) polystyrene at 220°C, Q = 0.0455 g/sec, V_L/V_0 = 501.7.

the drag force F_{drag}, and the rheological force F_{rheo}) was to evaluate the associated terms in the equation of motion.

It is seen in Tables III and IV that, in the spinning of high-density polyethylene and low-density polyethylene, contributions of both the inertial and drag forces are negligibly small compared to other components of force. This is attributable to the relatively low values of stretch ratio in those two materials. However, in the spinning of polystyrene which had a very high stretch ratio, contributions of both the inertial and drag forces are seen to be significant, as shown in Table V. Earlier, Ishibashi et al.[11] in their study of spinning nylon 6 also found that the contributions of the inertial and drag forces were significant.

Another interesting observation that may be made from the solution of eqs. (35) and (36) is the distribution of the axial velocity gradient (i.e., elongation rate), dv_z, dz, along the spinning way. Figure 11 gives representative profiles of dv_z, dz for comparison purposes. It should be noted that, for a given material, profiles of dv_z, dz would vary with stretch rate. Note also that in an earlier paper[1] the authors presented profiles of dv_z, dz for six fibers spun into an isothermal chamber. It is seen in Figure 11 that each material shows different behavior in the axial velocity gradient, far from the constant values much speculated on in earlier theoretical studies.

TABLE III
Force Distributions in a High-Density Polyethylene Threadline in Nonisothermal Spinning[a]

Distance, cm	F_{grav}, g	F_{inert}, g	F_{drag}, g	F_{rheo}, g
1.0	0.1058	0.0001	0.0165	7.4130
3.0	0.0811	0.0001	0.0238	7.3980
5.0	0.0698	0.0001	0.0288	7.3872
7.0	0.0625	0.0001	0.0329	7.3788
9.0	0.0571	0.0001	0.0365	7.3724
13.2	0.0485	0.0001	0.0429	7.3630
20.2	0.0396	0.0001	0.0505	7.3582
27.0	0.0335	0.0002	0.0537	7.4024
30.3	0.0313	0.0002	0.0535	7.4066
37.1	0.0275	0.0002	0.0500	7.4173

[a] $Q = 0.025$ g/sec; $V_0 = 1.598$ cm/sec; $V_L/V_0 = 8.16$; $T_0 = 220$°C.

TABLE IV
Force Distributions in a Low-Density Polyethylene Threadline in Nonisothermal Spinning[a]

Distance, cm	F_{grav}, g	F_{inert}, g	F_{drag}, g	F_{rheo} g
1.0	0.0697	0.0000	0.0047	0.3474
3.0	0.0519	0.0000	0.0068	0.3274
5.0	0.0401	0.0001	0.0095	0.3132
7.0	0.0318	0.0002	0.0127	0.3034
9.0	0.0258	0.0002	0.0163	0.2970
12.5	0.0186	0.0004	0.0232	0.2924
17.5	0.0124	0.0007	0.0332	0.3025
22.5	0.0085	0.0016	0.0413	0.3200
25.0	0.0071	0.0022	0.0433	0.3324
27.0	0.0060	0.0030	0.0426	0.3461

[a] $Q = 0.0247$ g/sec; $V_0 = 1.68$ cm/sec; $V_L/V_0 = 22.28$; $T_0 = 200$°C

TABLE V
Force Distributions in a Polystyrene Threadline in Nonisothermal Spinning[a]

Distance, cm	F_{grav}, g	F_{inert}, g	F_{drag}, g	F_{rheo}, g
1.0	0.0811	0.0004	0.0063	2.8697
3.0	0.0398	0.0017	0.0172	2.8532
5.0	0.0212	0.0052	0.0419	2.8529
7.0	0.0122	0.0137	0.0902	2.8699
9.0	0.0075	0.0315	0.1741	2.9123
12.5	0.0037	0.1041	0.4423	3.0916
17.5	0.0017	0.3983	1.1500	3.7071
22.5	0.0008	1.2851	2.2515	5.2149
27.6	0.0005	3.6999	3.3731	7.8046
30.1	0.0004	5.8000	3.4594	9.3881

[a] $Q = 0.0455$ g/sec; $V_0 = 2.17$ cm/sec; $V_L/V_0 = 501.78$; $T_0 = 220$°C.

Details of the heat transfer involved in melt spinning can also be obtained from the solutions of eqs. (35) and (36). Figure 12 gives predicted temperature profiles in fibers of polystyrene, low-density polyethylene, and high-density polyethylene. Note that these profiles are given just to demonstrate the reasonableness of the mathematical model developed in this

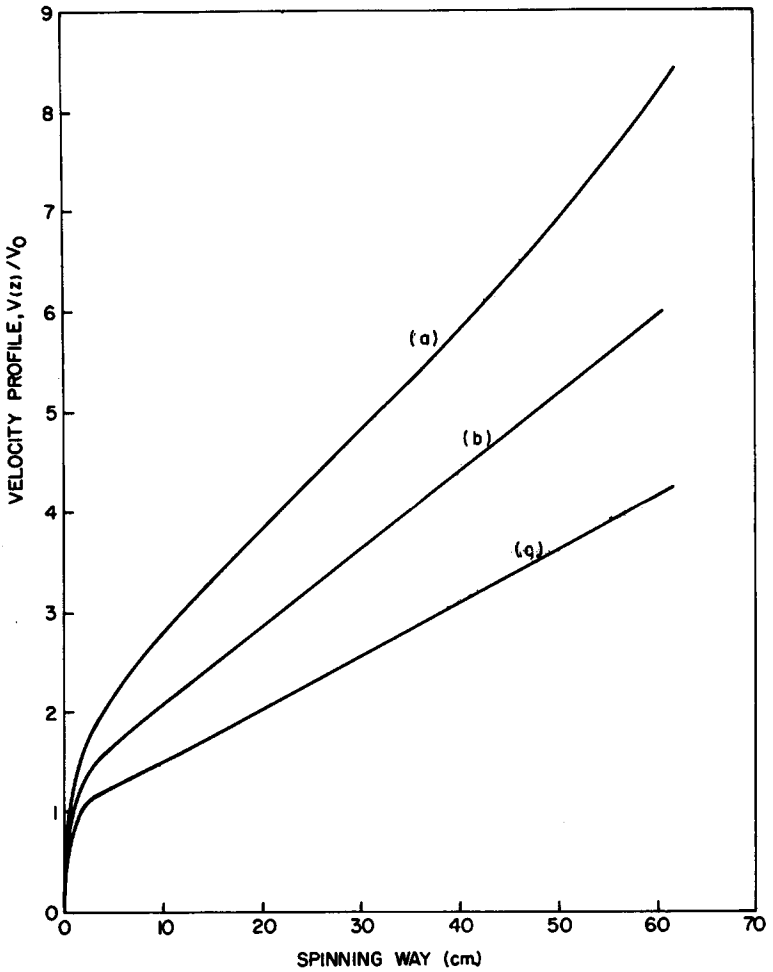

Fig. 8. Predicted velocity profiles in nonisothermal spinning of high-density polyethylene fibers for various stretch ratios: (a) $V_L/V_0 = 8.2$; (b) $V_L/V_0 = 6.1$; (c) $V_L/V_0 = 4.0$. Other spinning conditions: $Q = 0.025$ g/sec; $T_0 = 220$°C; $T_a = 25$°C.

paper. Space limitations here do not permit us to present simulation results investigating the effects of various parameters on the characteristics of heat transfer. Solution of eqs. (35) and (36) has enabled us to evaluate the effect of individual heat transfer mechanisms involved in cooling the molten threadlines.

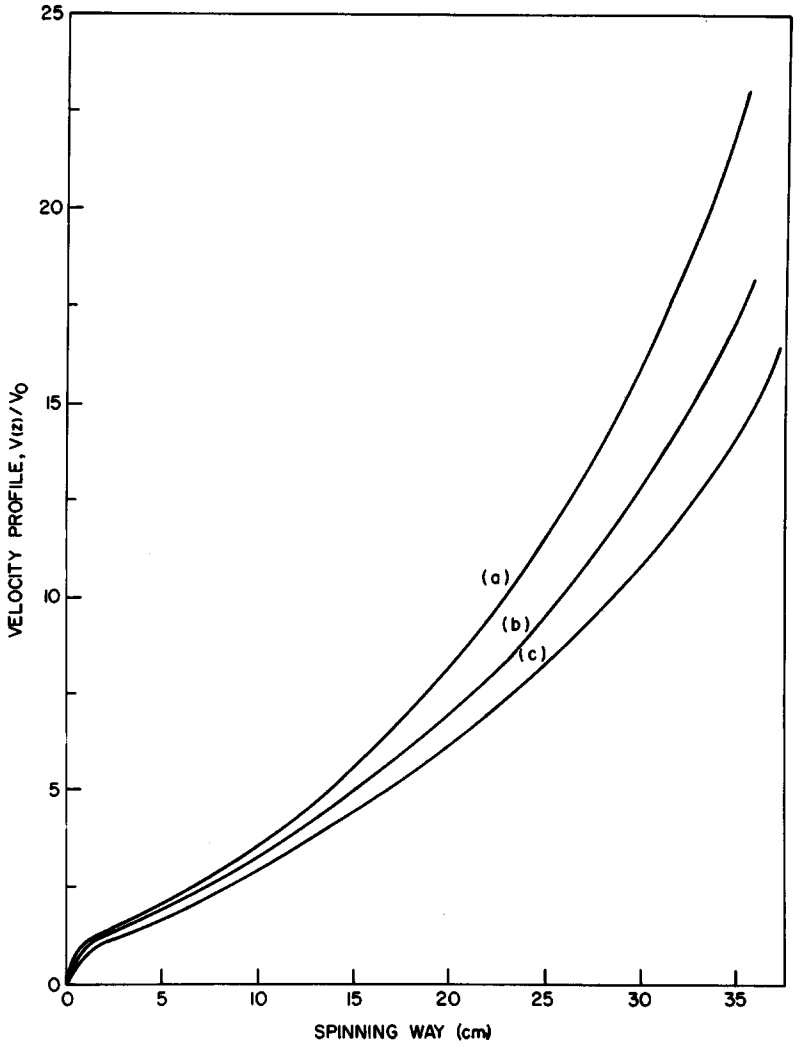

Fig. 9. Predicted velocity profiles in nonisothermal spinning of low density fibers for various stretch ratios: (a) $V_L/V_0 = 22.3$; (b) $V_L/V_0 = 17.4$; (c) $V_L/V_0 = 12.0$. Spinning conditions: $Q = 0.027$ g/sec; $V_0 = 1.68$ cm/sec; $T_0 = 200°C$; $T_a = 25°C$.

It has been found that the heat loss due to radiation accounts for (1) in high-density polyethylene fibers, approximately 30% of the total heat loss near the spinnerette and 10% as the fiber becomes solidified; (2) in low-density polyethylene fibers, approximately 20% of the total heat loss near the spinnerette and 2% as the fiber becomes solidified; (3) in polystyrene fibers, approximately 15% of the total heat loss near the spinnerette and less than 0.1% as the fiber becomes solidified. As may be surmised, these differences in the role of radiative heat transfer are attributable to the differences in stretch ratios for the materials investigated (see the spinning

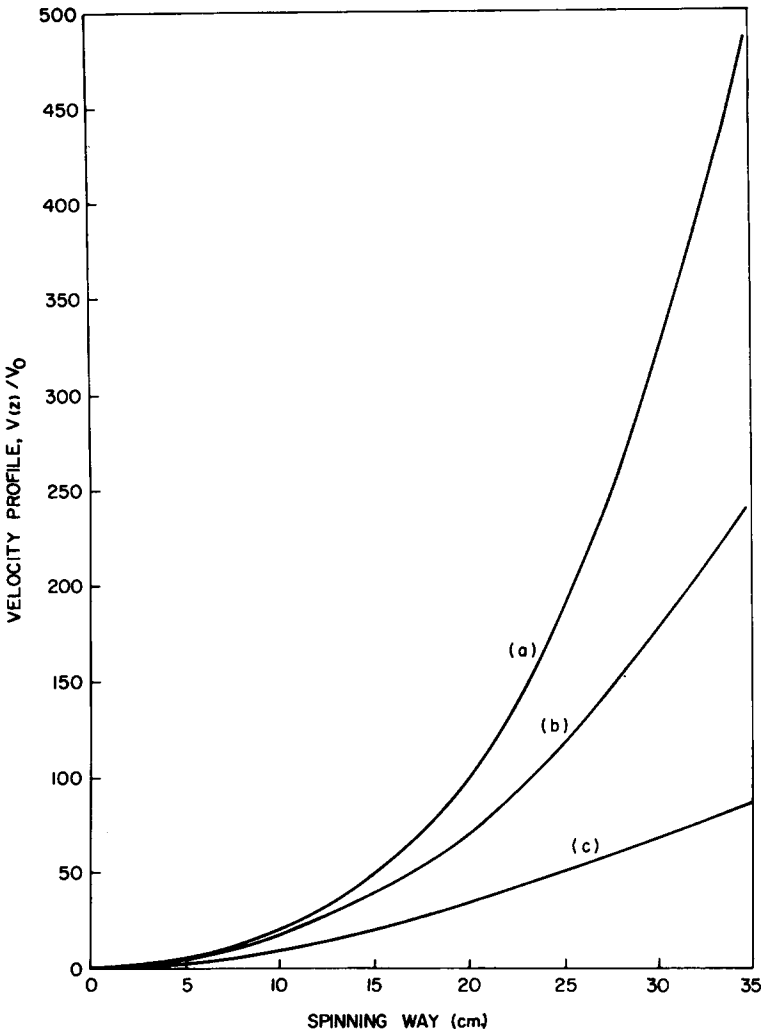

Fig. 10. Predicted velocity profiles in nonisothermal spinning of polystyrene fibers for various stretch ratios: (a) $V_L/V_0 = 501.7$; (b) $V_L/V_0 = 250.7$; (c) $V_L/V_0 = 100.0$. Other spinning conditions: $Q = 0.045$ g/sec; $T_0 = 220$°C; $T_a = 25$°C.

conditions given in Figs. 8 to 10). Earlier, Acierno et al.[8] also have taken into account the effect of radiation on the total rate of heat transfer in their study of spinning polystyrene and low-density polyethylene. They reported that radiation accounts for approximately 20% of the total heat loss near the spinnerette and 10% as the fiber solidifies. Considering the relatively low values of stretch ratio in their study, the predicted results of the heat loss due to radiation presented above are in good agreement. Acierno et al.[8] used actual measurements of fiber temperature along the spinning way in their estimation of the heat losses in melt spinning.

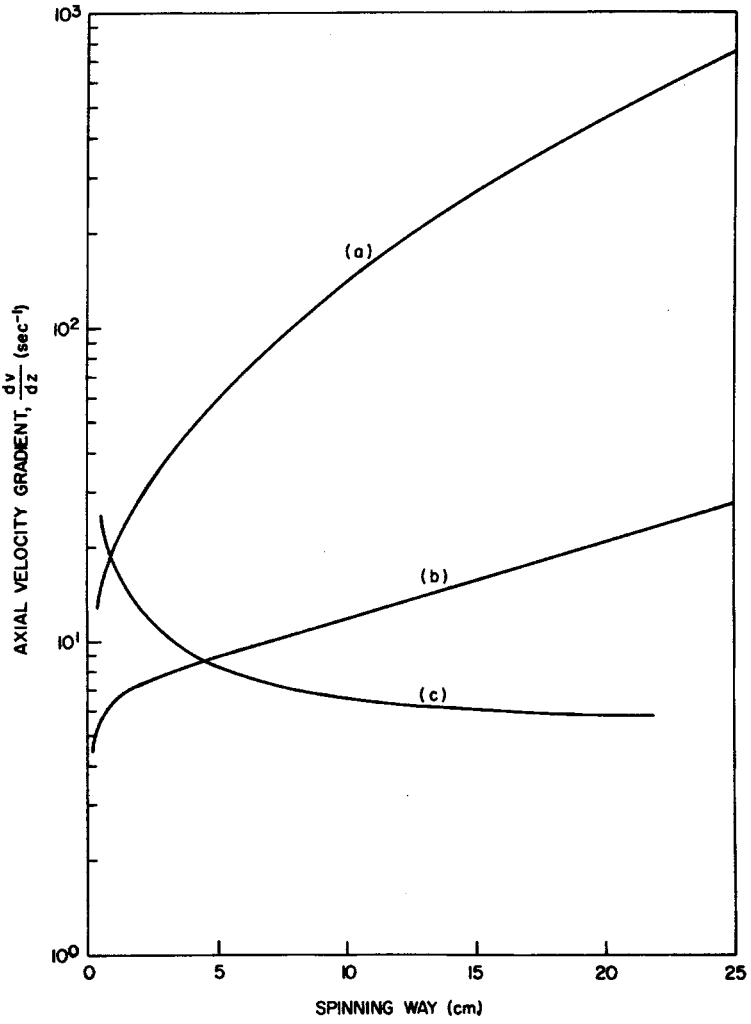

Fig. 11. Predicted elongation rate profiles in nonisothermal spinning: (a) polystyrene; (b) low-density polyethylene; (c) high-density polyethylene. Other spinning conditions same as those given in Figs. 8, 9, and 10.

It may be then concluded that in melt spinning at high stretch ratios, the effect of radiative heat transfer on the total heat loss while a filament is being stretched and cooled along the spinning way can be neglected, to all intents and purposes.

CONCLUSIONS

Based on the experimental data available in the literature of elongational viscosity of polymer melts, a generalized, empirical equation is proposed which takes into account the dependence of elongational viscosity on both

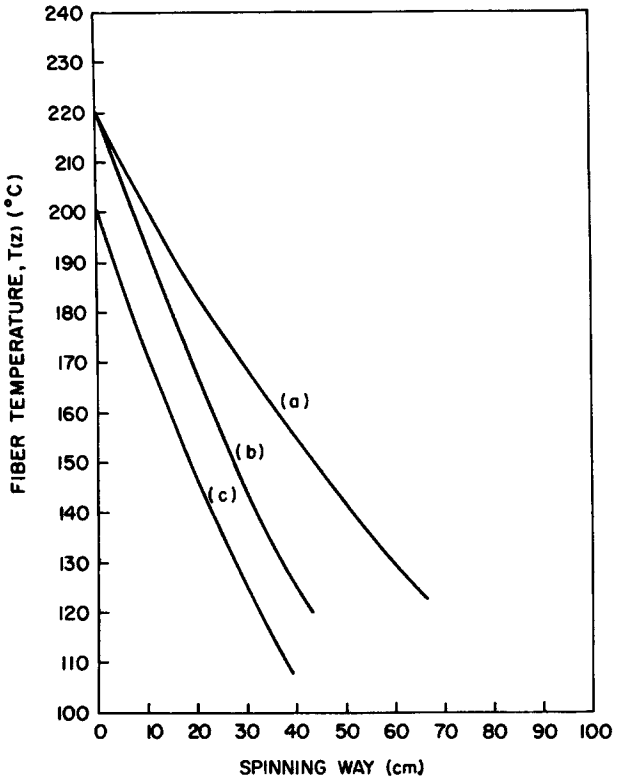

Fig. 12. Predicted temperature profiles in nonisothermal spinning: (a) high-density polyethylene; (b) polystyrene; (c) low-density polyethylene. Spinning conditions same as in Figs. 8, 9, and 10.

elongation rate and temperature. From this, a mathematical model for simulating the melt spinning process has been developed. The model has been tested against experimentally observed velocity profiles in fibers of polystyrene and high-density polyethyene spun into an isothermal chamber. It has been found that predicted velocity profiles agree well with experimentally observed ones. The mathematical model has been used to predict velocity and temperature profiles in fibers spun into a cooling medium. The simultaneous solution of momentum and energy balance equation by means of a numercial integration scheme has generated important information such as distributions of force components involved in spinning and distributions of the total rate of heat transfer along the spinning way. The analysis indicates that, as stretch ratio is increased, both the inertial and drag forces become increasingly important, whereas the contribution of radiative heat transfer to the total heat loss becomes negligibly small.

The work was supported in part by the National Science Foundation under Grant No. GK-23623.

References

1. C. D. Han and R. R. Lamonte, *Trans. Soc. Rheol.*, **16**, 447 (1972).
2. A. Ziabicki and K. Kedzierska, *Kolloid-Z.*, **171**, 51 (1960).
3. A. Ziabicki, *Kolloid-Z.*, **175**, 14 (1961).
4. E. H. Andrews, *Brit. J. Appl. Phys.*, **10**, 39 (1959).
5. A. Ziabicki and K. Kedzierska, *J. Appl. Polym. Sci.*, **6**, 111 (1962).
6. A. Ziabicki and K. Kedzierska, *J. Appl. Polym. Sci.*, **6**, 361 (1962).
7. M. E. Morrison, *A.I.Ch.E.J.*, **16**, 57 (1970).
8. D. Acierno, J. N. Dalton, J. M. Rodriguez, and J. L. White, *J. Appl. Polym. Sci.*, **15**, 2395 (1971).
9. S. Kase and T. Matsuo, *J. Polym. Sci. A*, **3**, 2541 (1965).
10. S. Kase and T. Matsuo, *J. Appl. Polym. Sci.*, **11**, 251 (1967).
11. T. Ishibashi, K. Aoki, and T. Ishii, *J. Appl. Polym. Sci.*, **14**, 1597 (1970).
12. M. J. Yamamoto, *J. Phys. Soc. Japan*, **12**, 1148 (1957).
13. A. S. Lodge, *Elastic Liquids*, Academic Press, New York, 1964.
14. J. L. White, *J. Appl. Polym. Sci.*, **8**, 1129 (1964); *ibid.*, 2339 (1964).
15. R. B. Bird and T. W. Spriggs, *Phys. Fluids*, **8**, 1390 (1965).
16. R. L. Ballman, *Rheol. Acta*, **4**, 1938 (1965).
17. J. Meissner, *Trans. Soc. Rheol.*, **16**, 405 (1972).
18. F. N. Cogswell, *Trans. Soc. Rheol.*, **16**, 383 (1972).
19. I. J. Chen, G. E. Hagler, L. E. Abbott, J. N. Dalton, D. C. Bogue, and J. L. White, *Trans. Soc. Rheol.*, **16**, 473 (1972).
20. F. N. Cogswell, *Rheol. Acta*, **8**, 187(1969).
21. F. T. Trouton, *Proc. Roy. Soc.*, **A77**, 426 (1906).
22. M. A. Matovich and J. R. A. Pearson, *Ind. Eng. Chem., Fundam.*, **8**, 512 (1969).
23. B. C. Sakiadis, *A.I.Ch.E.J.*, **7**, 26 (1961); *ibid.*, 221 (1961); *ibid.*, 467 (1961).
24. H. B. Keller, *Numerical Methods for Two-point Boundary-value Problems*, Blaisdell, Waltham, Mass., 1968.

Received May 25, 1972
Revised June 20, 1972